

# Overcoming Small Minirhizotron Datasets Using Transfer Learning

Weihuang Xu<sup>1</sup>, Guohao Yu<sup>1</sup>, Alina Zare<sup>1</sup>, Brendan Zurweller<sup>2</sup>, Diane Rowland<sup>3</sup>,  
Joel Reyes-Cabrera<sup>4</sup>, Felix B Fritsch<sup>4</sup>, Roser Matamala<sup>5</sup>, Thomas E. Juenger<sup>6</sup>

<sup>1</sup>Department of Electrical and Computer Engineering, University of Florida, FL, USA

<sup>2</sup>Department of Plant and Soil Science, Mississippi State University, MS, USA

<sup>3</sup>Department of Agronomy, University of Florida, FL, USA

<sup>4</sup>Division of Plant Sciences, University of Missouri, MO, USA

<sup>5</sup>Argonne National Laboratory, IL, USA

<sup>6</sup>Department of Integrative Biology, University of Texas at Austin, TX, USA

weihuang.xu@ufl.edu, azare@ufl.edu

## Abstract

Minirhizotron technology is widely used to study root growth and development. Automated analysis of root systems may facilitate new scientific discoveries that could be applied to address the world's pressing food, resource, and climate issues. A key component of automated analysis of plant roots from imagery is the automated pixel-level segmentation of roots from their surrounding soil. Supervised learning techniques appear to be an appropriate tool for the challenge due to varying local soil and root conditions. However, lack of enough annotated training data is a major limitation due to the error-prone and time-consuming manual labeling process. Transfer learning is a useful technique to help with training when available datasets are limited. Networks pre-trained on the ImageNet dataset are widely used due to its massive scale. However, because of poor relevance of the ImageNet dataset and limited target datasets, those pre-trained features may not work well in specific applications such as plant root segmentation. In this paper, we investigate the effect of pre-trained features from a massive-scale, irrelevant ImageNet dataset and a relatively moderate-scale, but relevant peanut root dataset on switchgrass root imagery segmentation applications. We compiled two minirhizotron image datasets to accomplish this study: one with 17,550 peanut root images and another with 28 switchgrass root images. Both datasets were paired with manually labeled ground truth masks. Deep neural networks based on the U-net architecture were used with different pre-trained features as initialization for automated, precise pixel-wise root segmentation in minirhizotron imagery. We observed that features pre-trained on a closely related but relatively moderate size dataset like our peanut dataset were more effective than features pre-trained on the

large but unrelated ImageNet dataset. We obtained 99% segmentation accuracy in switchgrass imagery using only 21 training images.

## 1. Introduction

Minirhizotron camera systems are a minimally-invasive imaging technology for monitoring and understanding the development of plant root systems[14]. A variety of root phenotypes can be determined from minirhizotron RGB root imagery, such as lengths, diameters, patterns and distributions at different depths. However, manually tracing roots in minirhizotron imagery is tedious and extremely time-consuming, which limits the number and size of experiments. Thus, techniques that can automatically and accurately segment roots from minirhizotron imagery are crucial to improve the efficiency of data collection and post-processing. A lot of efforts have been made to achieve this based on traditional methods [27, 28, 21] and modern deep learning methods [24, 23]. However, the performance of those methods are usually limited by the quantity and quality of the data, especially for the deep learning category.

Root segmentation belongs to the field of semantic image segmentation, which is one of the most challenging tasks in computer vision. Instead of assigning labels at the whole-image level for image classification problems, semantic image segmentation requires a model to predict a label for each pixel. Many methods based on deep convolutional neural networks (DCNN) have been proposed to address semantic segmentation tasks such as fully convolutional networks[13], SegNet[1], U-net[18], and deeplab[6]. Models based on the above methods have achieved success in segmentation of medical images[18, 15, 4, 29], satellite images[7, 16, 2], and plant images[5, 30]. Such segmenta-

tion models are based on supervised learning of large networks with a very large number of parameters, requiring a huge amount of data with ground truth to achieve a satisfactory performance. Deep neural networks trained on small datasets can quickly overfit for the small sets and perform poorly in larger unknown sets. Thus, a fundamental issue of using those models for many applications, including plant science, is limited availability of training data.

To address such problems, so-called transfer learning[10, 3] techniques have been developed that apply model-weights pre-trained on large-scale data as initial parameters, and then they fine-tune the models on target problems that usually have more limited training data. This process will work based on the assumption that those pre-trained features are fairly general and applicable to many visual image applications, and can be re-used for a different specific problem. When the target dataset is small, pre-trained features can significantly improve the performance and help with faster convergence. Leveraging this idea, features pre-trained on massive scale data such as ImageNet are widely used as initial weights in recent work, which achieved state-of-the-art results on a variety of different tasks, such as image classification[9, 20], object detection[10, 17, 19] and image segmentation[12, 5, 8]. However, more and more work is questioning the effects of ImageNet pre-training. Yosinski *et al.* [25] showed that features in shallow layers are more general and effective when transferred to other specific problem. On the contrary, features from higher layers are more problem-specific. Huh *et al.* [11] illustrated that transfer learning performance is similar with features pre-trained only on half of ImageNet dataset as opposed to the full dataset. ImageNet pre-training can help even less when it comes to discipline-specific research such as plant root studies, due to the lack of relevance of the ImageNet dataset relative to plant root datasets.

In this work, we collected a moderately sized peanut root minirhizotron imagery dataset and a small sized switchgrass root minirhizotron imagery dataset and manually traced root segments in both sets. We trained U-net based models with different depths on the peanut root dataset to achieve automated, precise pixel-wise root segmentation. We also investigated and compared the effect on segmentation performance of model depth to find an appropriate model depth for further transfer learning study. Then, we used a transfer learning approach to apply pre-trained features from the peanut root data and the ImageNet dataset on the small-scale switchgrass root dataset to explore the effect of different pre-trained features and the accuracy of segmentation. Based on this approach, we found that features pre-trained on a moderate-sized peanut dataset that was highly related to the target switchgrass dataset were more effective for our root segmentation problem than those pre-trained on the large-scale but less relevant ImageNet dataset.

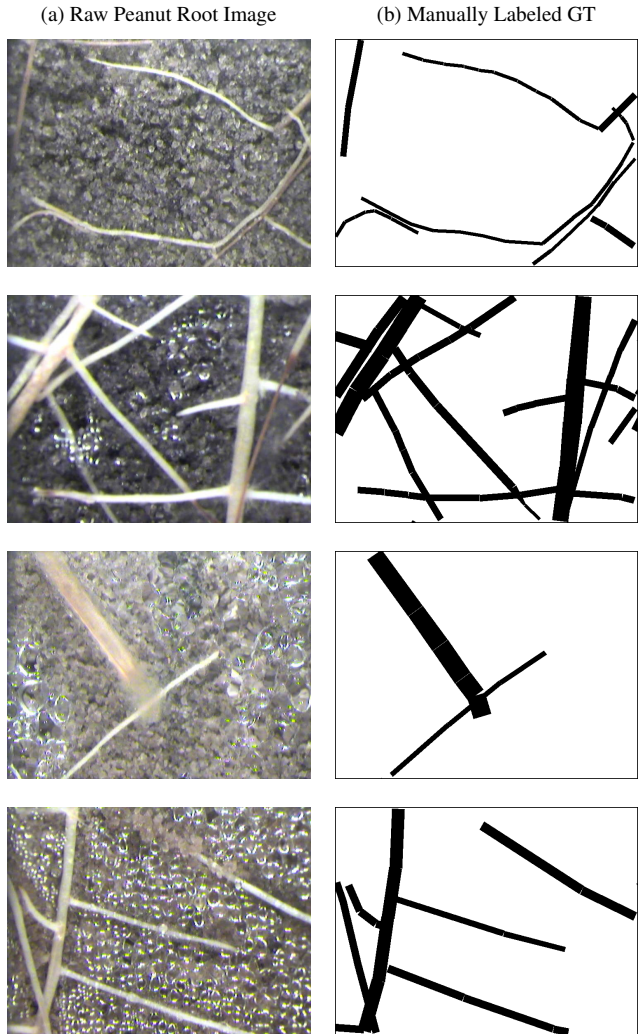


Figure 1. Examples of peanut root minirhizotron images (column (a)) captured by minirhizotron camera systems and manually labeled ground truth masks (column (b)) generated using WinRHIZO software.

In the following sections we describe our datasets, the semantic segmentation methods employed, our experiments using those methods with our datasets and other visual imagery datasets, and finally draw some conclusions based upon that work.

## 2. Datasets

We have compiled two minirhizotron root image datasets. The first dataset contains 17,550 peanut root RGB images and the second dataset has 17 switchgrass root RGB images. All images in both datasets were acquired using minirhizotron systems in the field, and were paired with manually labeled ground truth masks indicating the location of roots in each image. The details of data collection

and labelling process are as follows.

**Peanut root dataset** was collected in a field trial at the Plant Science Research and Education Unit (PSREU) during the 2016 growing season. Minirhizotron tubes 2 m in length were installed directly under and parallel to the row at a 45° angle to the soil surface after crop emergence using a hydraulic powered coring machine (Giddings Machine Company, Windsor, CO). After installation the portion of the minirhizotron tube protruding from the soil was covered with reflectance insulation (Reflectix Inc., Markleville, IN) to avoid root light exposure and precipitation from entering the tube. At each measurement date, images were captured at 13.5 mm increments (resulting typically in 112 image frames) along the minirhizotron tubes using a BTC 100X video camera and BTC I-CAP image capture software (Bartz Technology Corporation, Carpinteria, CA). Root parameter analysis was conducted using WinRHIZO Tron software (Regent Instruments Inc., Quebec, Canada) by hand tracing root segments within each image frame. The binary ground truth masks were generated by hand using the WinRHIZO Tron software package. The process consists of manually drawing different sizes of rectangles to highlight the area of roots while attempting to leave the soil blank. Examples of collected peanut root images and corresponding labeled ground truth masks are shown in Figure 1. Labelling by WinRHIZO is faster than labelling images pixel by pixel, since a large area of root pixels can be labeled at once. However, two shortcomings of this method are that: 1) the width of each rectangle is constant indicating that the roots in the labeled area have the same diameter, which is not true in practice; and 2) when the roots are not straight, there are gaps between labeled regions and the labeled edges of roots are not smooth.

**Switchgrass root dataset** was collected using a CI-602 in-situ root imager (CID Bio- Science, Camas, WA, USA) in minirhizotron tubes in a 2-year old switchgrass field at the U.S. Department of Energy National Environmental Research Park at Fermilab in Batavia, IL, USA. Minirhizotron tubes were installed with an angle of 60° to the soil surface to an approximate maximum vertical depth of 120 cm using an angled guided soil core sampler. Foam caps were installed to eliminate root light exposure, reduce temperature variation in the root zone, and stop precipitation from entering the tubes. Root images were taken at 300 dots per inch (11.8 pixels per millimeter) from eight depth intervals along the minirhizotron tubes. All the binary ground truth masks were manually labeled on superpixel level[26]. Examples of raw switchgrass images and corresponding ground truth masks are shown in Figure 2.

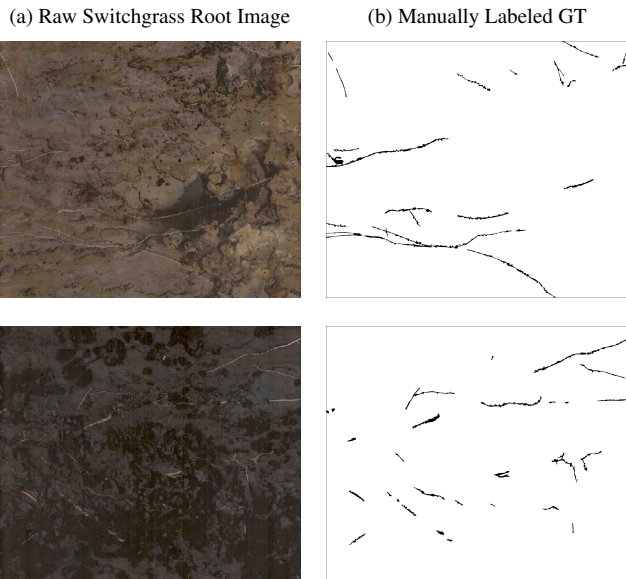


Figure 2. Examples of switchgrass root images (column (a)) captured by minirhizotron camera systems and manually labeled ground truth masks (column (b)).

## 3. Methods

### 3.1. Network Architecture

A U-Net[18] based encoder-decoder neural network was used for root segmentation. The network architecture is shown in Figure 3. The left half of the architecture works as an encoder where each block consists of two 3x3 convolution layers followed by one 2x2 max-pooling layer to down sample feature maps. The right half of the architecture works as a decoder where each block consists of one transpose convolution layer and two 3x3 convolution layers. The transpose convolution layer up-samples the size of feature maps by two. The encoder blocks are trained to extract dense feature maps from minirhizotron RGB imagery. Via skip connections, those feature maps will be concatenated with higher-level ones in corresponding decoders to offer more spatial information in output mask. The last layer is a 1x1 convolution layer (i.e., a weighted sum across all feature layers) to convert feature maps to a heat map. Then, the softmax function is used to assign class labels to each pixel. As it uses fully convolutional network architecture [13], a U-Net can be trained end-to-end with input images of any size. In order to keep the dimension of the output segmentation mask to be the same as input images, zero padding is used in every convolution layer. The model was implemented using the Pytorch library(1.1.0) and trained on a GTX 1080TI GPU with 12GB of RAM.

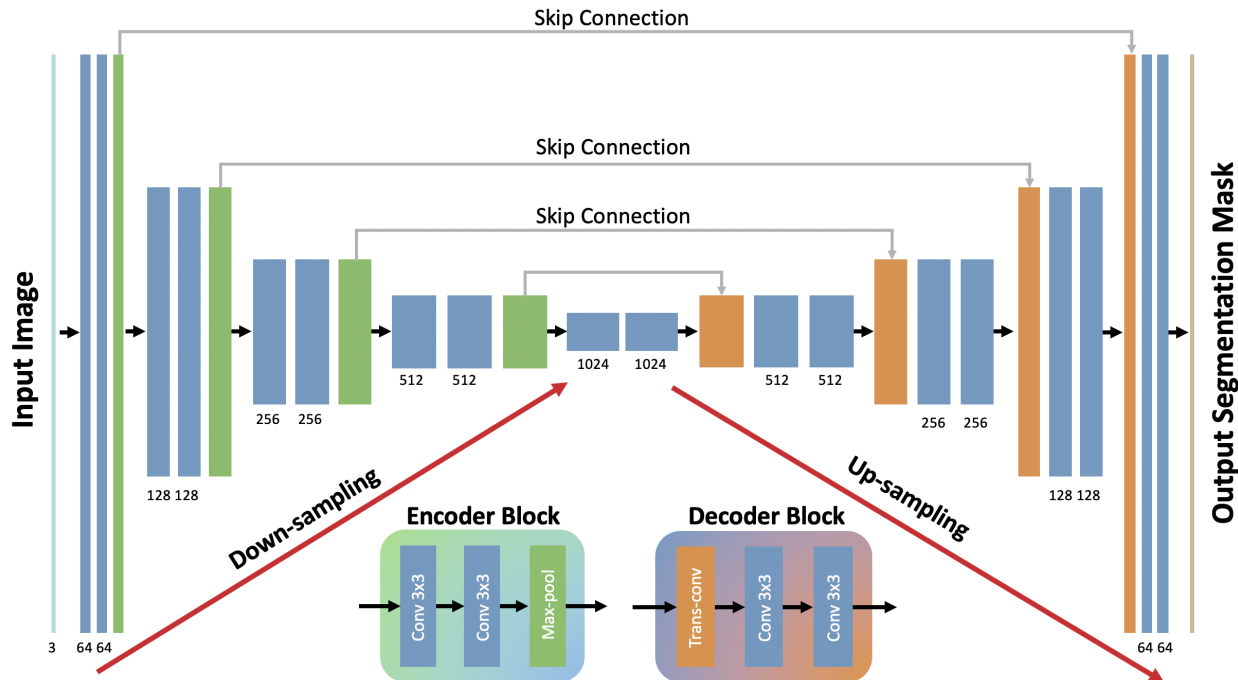


Figure 3. An illustration of the U-Net based encoder-decoder architecture. Each encoder block consists of two 3x3 convolution layers with ReLU (blue rectangle) and one 2x2 max-pooling layer (green rectangle). Each decoder block consists of one transpose convolution layer (orange rectangle) and two 3x3 convolution layers. The number of output channels of each convolution layer is denoted at the bottom of each blue rectangle. Feature maps extracted from encoders are concatenated to the corresponding decoder via skip connection. A 1x1 convolution layer is used at the end to reduce the number of channels.

### 3.2. Evaluation Metrics

The neural network will generate probability score for each pixel, representing the likelihood of a pixel belonging to the root class. The quality of the binary segmentation mask is sensitive to probability thresholds which usually vary for different models. The receiver operating characteristic (ROC) curve shows the tradeoff between the true positive rate (TPR) and the false positive rate (FPR) for different thresholds. The value of the area under the curve (AUC) is usually calculated from ROC curves to evaluate overall classification performance (both root pixels and non-root pixels) using different probability thresholds. The perfect score of AUC in ROC curve is 1, which indicate 100% classification accuracy on all pixels. The number of root pixels and non-root pixels are heavily unbalanced in our switchgrass root images. The TPR will easily reach 1 at small FPR, even when a relatively large amount of non-root pixels are mis-classified. Thus, it is difficult to evaluate the classification accuracy of root class on switchgrass root images based on ROC curves, because the overall classification accuracy will be overwhelmed by the classification accuracy for non-root pixels. Therefore, we plotted the precision-recall (PR) curves to help evaluate the classification per-

formance of root pixels specifically. The PR curves show the tradeoff between the precision and recall for different thresholds. Recall is the same as TPR indicating the percentage of correctly classified root pixels over all root pixels. Precision indicates the percentage of true root pixels over all the root pixels the model predicted. A higher AUC value for a PR curve shows that the model is more likely to make accurate prediction on root pixels. In our experiments, TPR (recall), FPR and precision values were calculated at the pixel-level by comparing the output predicted mask to the manually labeled ground truth.

### 4. Experiments and Results

We first trained our model on the peanut root dataset to investigate the segmentation performance on plant root minirhizotron imagery when moderate-sized dataset is available. Then, we designed experiments to demonstrate how the pre-trained features can help improve segmentation performance when a limited switchgrass dataset is used. We also compared the effect of features pre-trained on well-known massive scale ImageNet dataset and features pre-trained on our peanut root dataset.

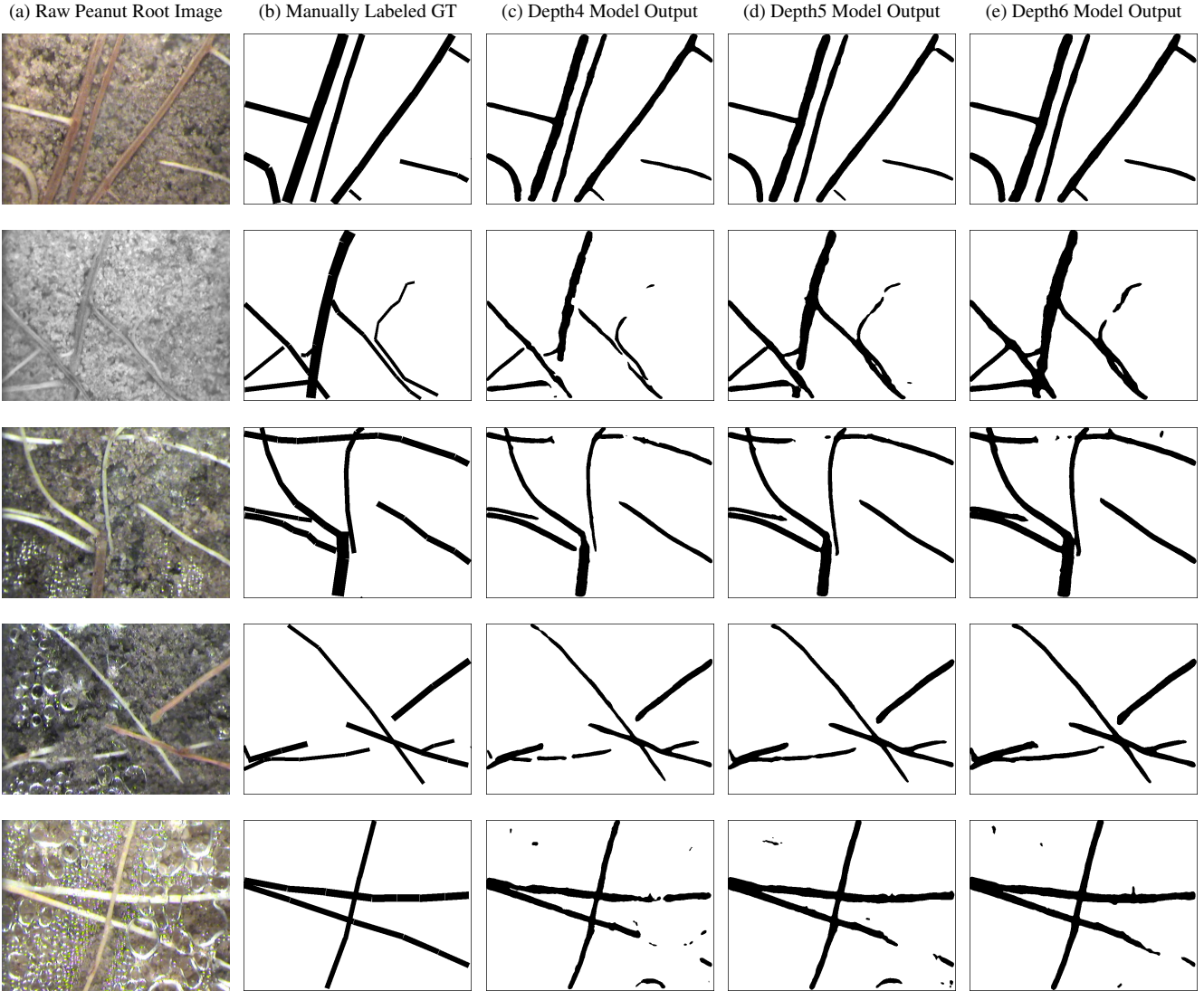


Figure 4. Segmentation results of selected test images taken across differing depths, dates, and local environments. Column (a) shows raw input peanut root minirhizotron images. Column (b) shows the manually labeled ground truth masks. Columns (c)-(e) show the segmentation results of models with depth 4, 5 and 6, respectively.

#### 4.1. Segmentation Performance on Peanut Root Dataset

**Experiment setup.** Model depth is crucial to the performance, especially when the training data is limited. Deeper networks can extract higher-level features to improve segmentation performance, but it is easier to overfit on small training datasets. To find the proper model depth for our peanut root dataset and future use on transfer learning experiment on switchgrass dataset, we implemented three models with depth 4, depth 5 and depth 6, where model depth refers to the number of encoders and decoders in the down-sampling and up-sampling path. The peanut root im-

ages were collected across different dates, tubes and depths. In order to ensure that the testing data and training data share the same distribution, we randomly picked 90% of the images from each date, tube and depth for training and the remaining 10% for testing. The inputs to the model were entire images (instead of stacking small randomly selected patches). The model was trained end-to-end from scratch using the SGD optimizer with learning rate 0.0001 and momentum 0.8. We set the batch size to be two due to GPU memory limitation and used binary cross-entropy as loss function. All models were trained for 100 epochs for five trials with different randomly initialized parameters. We plotted ROC curves for each model and calculated average

AUC values and standard deviation of AUC values based on five trials.

**Experimental results.** The segmentation results of the three models with different depths are shown in Figure 4. Column (a) shows the raw peanut root images taken from the minirhizotron system. These images were taken across differing depths, dates, and local environments. The corresponding manually labeled ground truth masks are shown in column (b). Column (c)-(e), show segmentation masks of our models with depth 4, depth 5 and depth 6, respectively. Global threshold was set to be 0.5 to generate the binary segmentation mask. Qualitatively, all three models provided good segmentation results. Most of the roots can be segmented from complicated soil backgrounds. Our method solved two major issues caused by the manual labelling process using WinRHIZO software, those of fixed label width along rectangles, and gaps between neighboring rectangles. Our model can capture the real thickness and diameter variation along each root. The segmented roots are consistent and smooth instead of having a boxy shape with gaps in manually labeled ground truth masks. As shown in column (c)-(e), our segmentation masks have a better representation of roots, which can with accurate determination of root traits in subsequent measurements.

Some interesting details were observed in the segmentation results in the last three rows in Figure 4. In the third row, part of the top of the root is covered by soil in the raw peanut root image. An example of the robustness of our method is that a small area of the ground truth mask was mislabeled; however, our method obtained the correct answer in all three models. In the fourth row, the root at the bottom left of the picture is partially covered by soil. We expected that it would be considered as a single piece of root as it was labeled as such in the ground truth mask. The shallow model (depth 4) generated three separated small pieces of root instead of one unbroken piece. In contrast, deeper models (depth 5 and depth 6) were capable of filling the gap and generated an unbroken root. This ability is very important when considering the density or number of roots in a specific area. The last row shows the case of a very complicated background. Because of a wide variety of reflections, it is very difficult to eliminate water bubbles in segmentation results. Our method was able to remove most of the water bubbles, but there still was some residual noise in the segmentation results. The output masks from depth 6 model are much cleaner than depth 5 and depth 4 models, which indicates that the deeper network is more powerful to accommodate complex noise in order to match ground truth masks as close as possible. This is reasonable, because a deeper network can extract higher-level features to further improve the reconstruction step in decoders.

In order to evaluate the consistency of the models, we trained each model 100 epochs for five trials with differ-

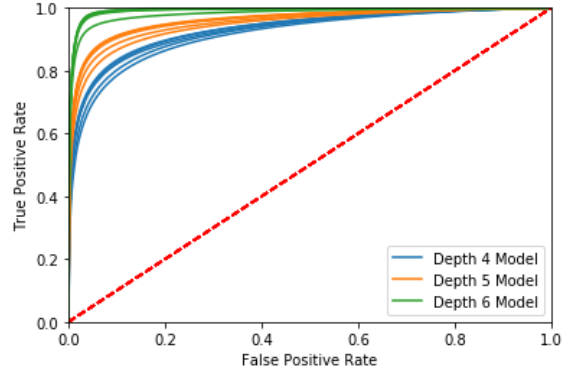


Figure 5. ROC curves plotted for models with depth 4 (Blue), depth 5 (Orange), and depth 6 (Green), respectively. Each model was trained five times with random weight initialization.

Table 1. Average AUC and standard deviation of AUC calculated from ROC curves for different models

Model	Average AUC $\pm$ Std. AUC
Depth 4	$0.9259 \pm 0.007$
Depth 5	$0.9565 \pm 0.007$
Depth 6	$0.9904 \pm 0.005$

ent random weight initialization. We calculate the TPR and FPR using the entire test dataset containing 0.7 billion pixels. The ROC curves for each model are shown in Figure 5. The average and Std. of AUC for each model are shown in Table 1. The depth 6 model had the highest average AUC of 0.9904 indicating the best segmentation accuracy among all the models. Additionally the method showed good consistency as all three models had small variance in AUC.

## 4.2. Transfer Learning on Limited Switchgrass Root Dataset

**Experiment setup.** We designed experiments on the small-scale switchgrass root dataset to explore the effect of pre-trained features from popular massive-scale ImageNet dataset and our own peanut root dataset. Compared with the ImageNet dataset that has 14 million images, our peanut root dataset is quite small, but much more relevant to the switchgrass root dataset. As the goal in this experiment is to figure out the role of pre-trained features on a general model instead of finding the highest performing network architecture, we implemented the U-net based model with down path architecture the same as the VGG13 network[22]. Besides the features in the encoder, decoder blocks also extract higher-level feature maps for up-sampling. We believe those feature maps are also crucial for improving segmentation performance as in the limited switchgrass root dataset.

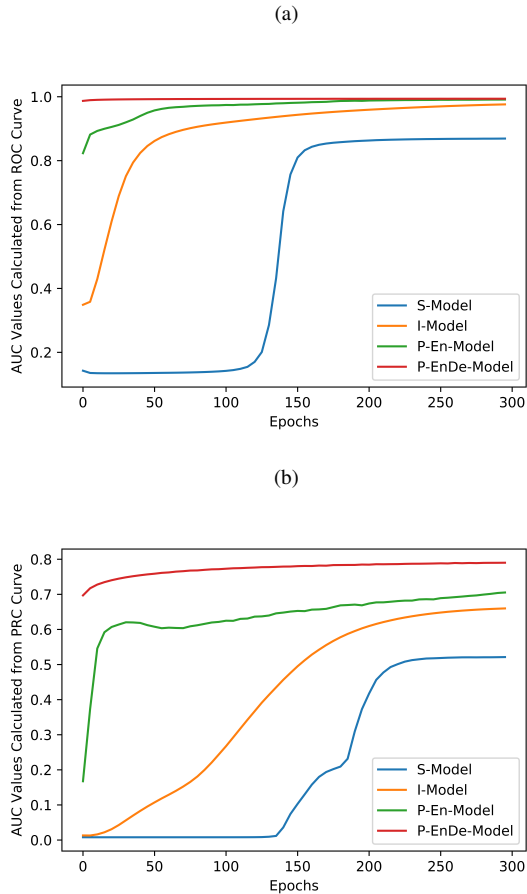


Figure 6. AUC values for (a) ROC curves and (b) PR curves at each training epoch for all the models with different weight initialization. Blue curve: S-model, weights in both encoder and decoder are randomly initialized. Orange curve: I-model, weights in encoder are initialized with ImageNet pre-trained features and randomly initialized weights in decoder. Green curve: P-En-model, weights in encoder are initialized with peanut pre-trained features and randomly initialized weights in decoder. Red curve: P-EnDe-model, weights in both encoder and decoder are initialized with peanut pre-trained features.

Thus, we studied pre-trained features not only in encoder, but also in the combination of encoder and decoder. To make a comprehensive comparison of different pre-trained features, we implemented four models namely: 1) S-model whose weights are randomly initialized; 2) I-model whose encoder is initialized with pre-trained weights on ImageNet dataset; 3) P-En-model whose encoder is initialized with pre-trained weights on our peanut dataset; and 4) P-EnDe-model whose encoder as well as decoder are initialized with pre-trained weights on our peanut dataset. These four models have exactly the same architecture but different weight initialization. The S-model works as base-line model in the comparison. All the models were trained on the switchgrass

dataset for 300 epochs. We used a relatively larger learning rate  $5e^{-5}$  for the S-model, because it was trained from scratch and a smaller learning rate of  $1e^{-5}$  for the I-model, P-En-model and P-EnDe-model. Since randomly initialized weights can cause variance in segmentation results, each model was trained five times to compare the performance consistency. To make sure the evaluation is accurate, we used 7 well-annotated switchgrass minirhizotron images for evaluating the performance of each model and the remaining 21 images for training. Due to the limitation of GPU memory, each switchgrass root image was evenly cropped into 15 small images with size 720x510 pixels. Since the number of root pixels and the number of background pixels were highly imbalanced, we set positive weight of root pixels as 20 in binary-cross entropy loss function to prevent models from heavily biasing towards the large number of non-root pixels.

**Experimental results.** As shown in Figure 6, the AUC values based on the ROC curves and PR curves were calculated for all models at each training epoch. AUC values calculated from ROC curves indicate the segmentation accuracy on both root pixels and soil pixels. According to Figure 6 (a), starting from the very beginning, models with pre-trained features had higher AUC values than the S-model that was trained from scratch. Under the same training condition, pre-trained features improved the overall segmentation performance substantially. Specifically, features pre-trained on the peanut root dataset were more effective than features pre-trained on ImageNet dataset, even though the ImageNet dataset is much larger than the peanut dataset. PR curves show classification performance on root class. High AUC values in PR curves represent both high precision and recall values, indicating that features are more effective to classify root pixels. P-En-model and P-EnDe-model had higher AUC values, which proves that peanut pre-trained features are more helpful than ImageNet pre-trained features for switchgrass root segmentation. Additionally, models with pre-trained features converged faster, especially the P-EnDe-model with both pre-trained encoder and decoder on peanut dataset.

We selected two switchgrass root images with the best manually labeled ground truth to show binary segmentation masks generated by one of each of the four models at epoch 10, 100, 200 and 300 as shown in Figure 7. The quality of the binary segmentation mask is sensitive to probability thresholds which usually vary for different models. To make a fair comparison, we plotted ROC curves for each model at different epochs and picked threshold corresponding to the FPR value at 1%. The FPR value was calculated based on all test images, but it could vary for each individual image. Due to the limited dataset, the S-model could not classify roots until several hundreds epochs. Also, a lot of non-root pixels were mis-classified (false positive) in

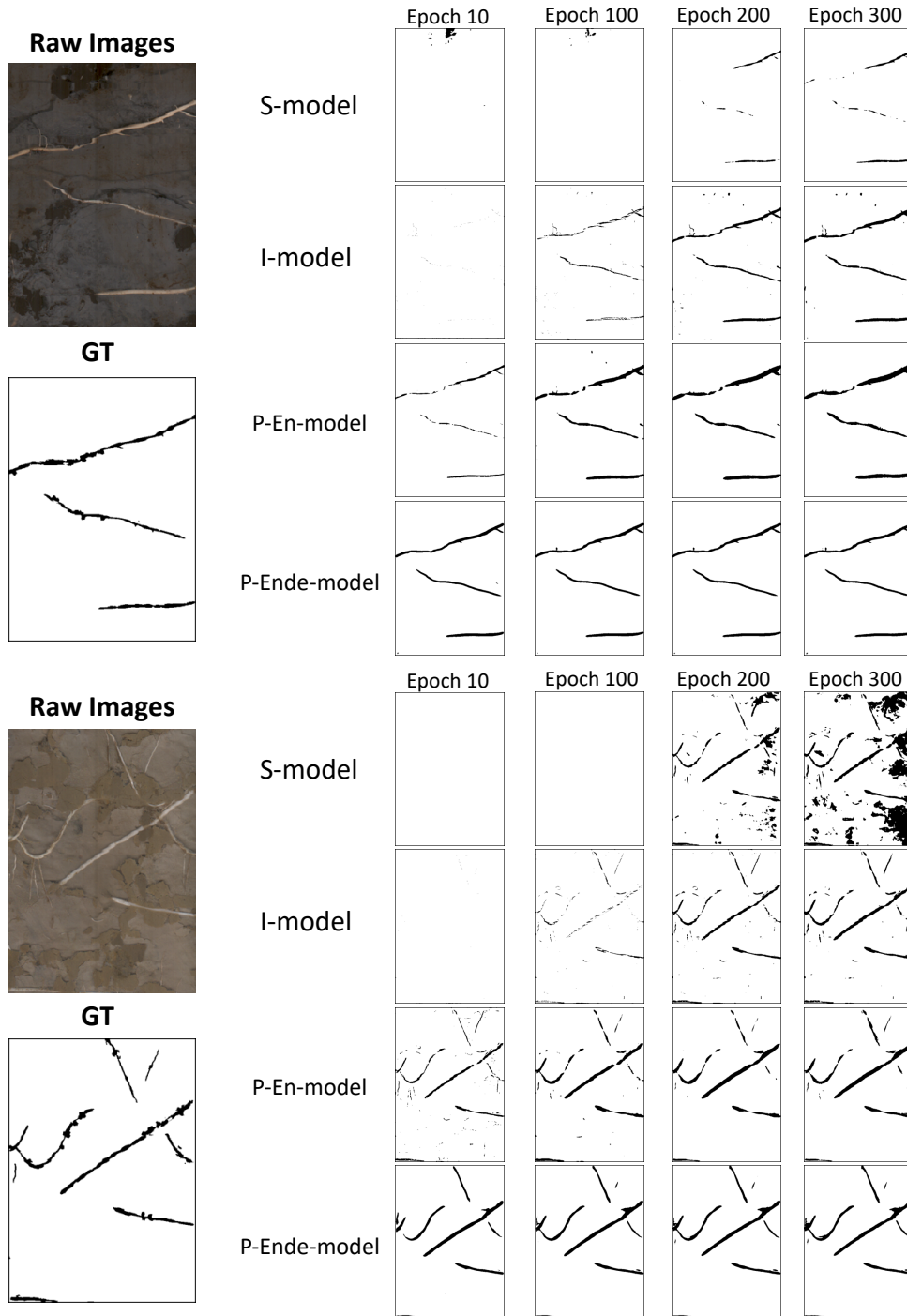


Figure 7. Segmentation results of selected test images generated by S-model, I-model, P-En-model and P-EnDe-model at epoch 10, 100, 200 and 300.

the segmentation results. The I-model performed a bit better than the S-model, but not as good as the P-En-model and P-EnDe-model. Qualitatively, the P-EnDe-model had the best contrast ratio between root pixel values and background soil pixel values, which represents the best capa-

bility to accurately segment roots from complicated backgrounds. Additionally, even at epoch 10, the P-EnDe-model already had decent segmentation performance, indicating that peanut pre-trained features were more effective than ImageNet pre-trained features.



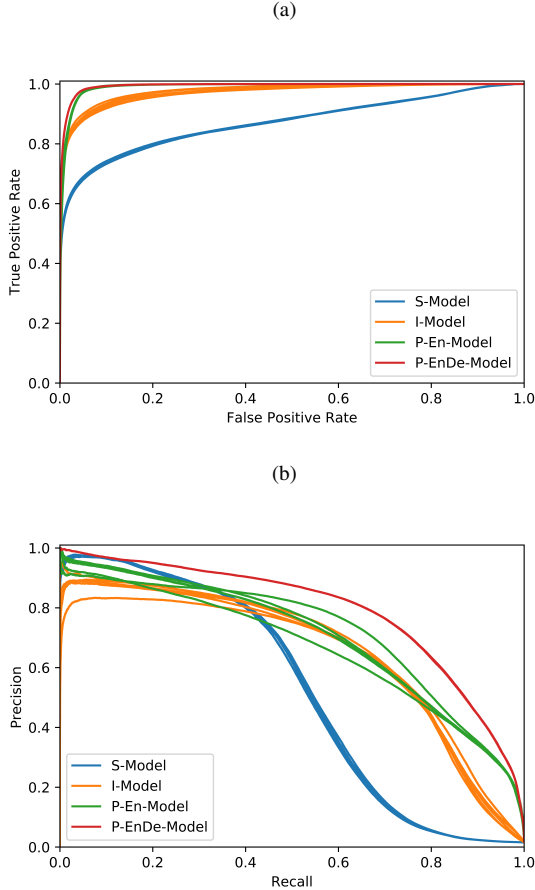


Figure 8. (a) ROC curves and (b) PR curves for S-model, I-model, P-En-model and P-EnDe-model at epoch 300.

Figure 8 shows the ROC and PR curves for each model (5 trials for each model) at the 300 epoch. The average and standard deviation value of the AUC among those 5 trials are shown in Table 2. Models used with the peanut-pre-trained encoder were more consistent (lower standard deviation of AUC on ROC curve) than models used with the ImageNet encoder. The S-model had a poor precision score when recall was close to 1, which indicates that a comparable amount of soil pixels were mis-classified as root. Furthermore, the P-En-model and P-EnDe-model with peanut pre-trained features offered much higher precision scores when recall was close to 1, which proves that the peanut features were more relevant to roots instead of soil. Also, the P-EnDe-model had the highest average AUC values on both ROC and PR curves indicating that pre-trained features in the decoder also were important for segmentation tasks.

## 5. Discussion

Our results show that pre-trained features improve the segmentation performance when a limited dataset is avail-

Table 2. Average AUC and standard deviation of AUC calculated from ROC and PR curves for different models

Model	Average AUC $\pm$ Std. AUC	
	ROC Curves	PR Curves
S-model	$0.870 \pm 0.001$	$0.525 \pm 0.003$
I-model	$0.973 \pm 0.004$	$0.652 \pm 0.008$
P-En-model	$0.991 \pm 0.000^a$	$0.700 \pm 0.020$
P-EnDe-model	<b><math>0.994 \pm 0.000^b</math></b>	<b><math>0.790 \pm 0.000^c</math></b>

Only three significant digits are shown in the table. The actual value is: <sup>a</sup> 0.0004, <sup>b</sup> 0.00005 and <sup>c</sup> 0.0004

able. Also, the pre-trained features can help a model converge faster and thus save a large amount of training time. However, (perhaps, intuitively) pre-trained features from a massive-scale dataset are not always the best for imagery with different visual appearances. Although the size of a pre-trained dataset is important, it appears that the relevance of the pre-trained with respect to the target dataset is more crucial for segmentation performance. If those two datasets are very different, only the features in shallow layers can help with segmentation results, since low-level features are more general such as edges or textures[25]. The higher-level features are more problem-specific, which could mislead the decision of a model on the target dataset. This is even more pronounced when the model is deeper, because the proportion of effective parameters in shallow layers is getting smaller. In contrast, features from a dataset that is small but highly related to the target dataset are more valuable regardless of how deep the model is, because both low-level and high-level features are useful to the target dataset.

## 6. Conclusions

In this work, we propose the use of U-net based deep neural networks for automated, precise, pixel-wise segmentation of plant roots in minirhizotron imagery. Our model achieved high quality segmentation masks with 99.04% accuracy at the pixel-level and overcame errors in human-labeled ground truth masks. We also found that deep networks can better resolve more challenging images (more complicated backgrounds) than shallow networks. Furthermore, we improved the segmentation performance on a small-scale switchgrass root dataset by using pre-trained features from the massive-scale ImageNet dataset and a mid-scale peanut root dataset, followed by fine tuning on a small switchgrass root dataset. We obtained above 99% segmentation accuracy in switchgrass root segmentation with pre-trained encoder and decoder from our peanut root dataset. Our results indicate that both pre-trained encoder and decoder can help with segmentation performance when the target dataset is small. Also, features pre-trained on a

dataset that is relatively small but highly related to the target dataset were more effective than those pre-trained on a massive-scale but less relevant dataset.

## Acknowledgement

This work was partially supported by U.S. Department of Energy, Office of Science, Office of Biological and Environmental Research award number DE-SC0014156. The information, data, or work presented herein was partially funded in part by the Advanced Research Projects Agency-Energy (ARPA-E), U.S. Department of Energy, under Award Number DE-AR0000820. The views and opinions of authors expressed herein do not necessarily state or reflect those of the United States Government or any agency thereof.

## References

- [1] V. Badrinarayanan, A. Kendall, and R. Cipolla. Segnet: A deep convolutional encoder-decoder architecture for image segmentation. *arXiv preprint arXiv:1511.00561*, 2015. 1
- [2] Y. Bai, E. Mas, and S. Koshimura. Towards operational satellite-based damage-mapping using u-net convolutional network: A case study of 2011 tohoku earthquake-tsunami. *Remote Sensing*, 10(10):1626, 2018. 1
- [3] Y. Bengio. Deep learning of representations for unsupervised and transfer learning. In *Proceedings of ICML Workshop on Unsupervised and Transfer Learning*, pages 17–36, 2012. 2
- [4] H. Chen, X. Qi, L. Yu, Q. Dou, J. Qin, and P.-A. Heng. Dcan: Deep contour-aware networks for object instance segmentation from histology images. *Medical image analysis*, 36:135–146, 2017. 1
- [5] J. Chen, Y. Fan, T. Wang, C. Zhang, Z. Qiu, and Y. He. Automatic segmentation and counting of aphid nymphs on leaves using convolutional neural networks. *Agronomy*, 8(8):129, 2018. 1, 2
- [6] L.-C. Chen, G. Papandreou, I. Kokkinos, K. Murphy, and A. L. Yuille. Deeplab: Semantic image segmentation with deep convolutional nets, atrous convolution, and fully connected crfs. *IEEE transactions on pattern analysis and machine intelligence*, 40(4):834–848, 2018. 1
- [7] A. Constantin, J.-J. Ding, and Y.-C. Lee. Accurate road detection from satellite images using modified u-net. In *2018 IEEE Asia Pacific Conference on Circuits and Systems (APCCAS)*, pages 423–426. IEEE, 2018. 1
- [8] J. Dai, K. He, and J. Sun. Instance-aware semantic segmentation via multi-task network cascades. In *Proceedings of the IEEE Conference on Computer Vision and Pattern Recognition*, pages 3150–3158, 2016. 2
- [9] J. Donahue, Y. Jia, O. Vinyals, J. Hoffman, N. Zhang, E. Tzeng, and T. Darrell. Decaf: A deep convolutional activation feature for generic visual recognition. In *International conference on machine learning*, pages 647–655, 2014. 2
- [10] R. Girshick, J. Donahue, T. Darrell, and J. Malik. Rich feature hierarchies for accurate object detection and semantic segmentation. In *Proceedings of the IEEE conference on computer vision and pattern recognition*, pages 580–587, 2014. 2
- [11] M. Huh, P. Agrawal, and A. A. Efros. What makes imagenet good for transfer learning? *arXiv preprint arXiv:1608.08614*, 2016. 2
- [12] V. Iglovikov and A. Shvets. Terausnet: U-net with vgg11 encoder pre-trained on imagenet for image segmentation. *arXiv preprint arXiv:1801.05746*, 2018. 2
- [13] J. Long, E. Shelhamer, and T. Darrell. Fully convolutional networks for semantic segmentation. In *Proceedings of the IEEE conference on computer vision and pattern recognition*, pages 3431–3440, 2015. 1, 3
- [14] H. Majdi. Root sampling methods-applications and limitations of the minirhizotron technique. *Plant and Soil*, 185(2):255–258, 1996. 1
- [15] R. K. Pandey, A. Vasani, and A. Ramakrishnan. Segmentation of liver lesions with reduced complexity deep models. *arXiv preprint arXiv:1805.09233*, 2018. 1
- [16] A. Rakhlin, A. Davydov, and S. Nikolenko. Land cover classification from satellite imagery with u-net and lovász-softmax loss. In *2018 IEEE/CVF Conference on Computer Vision and Pattern Recognition Workshops (CVPRW)*, pages 257–2574. IEEE, 2018. 1
- [17] S. Ren, K. He, R. Girshick, and J. Sun. Faster r-cnn: Towards real-time object detection with region proposal networks. In *Advances in neural information processing systems*, pages 91–99, 2015. 2
- [18] O. Ronneberger, P. Fischer, and T. Brox. U-net: Convolutional networks for biomedical image segmentation. In *International Conference on Medical image computing and computer-assisted intervention*, pages 234–241. Springer, 2015. 1, 3
- [19] P. Sermanet, D. Eigen, X. Zhang, M. Mathieu, R. Fergus, and Y. LeCun. Overfeat: Integrated recognition, localization and detection using convolutional networks. *arXiv preprint arXiv:1312.6229*, 2013. 2
- [20] A. Sharif Razavian, H. Azizpour, J. Sullivan, and S. Carlsson. Cnn features off-the-shelf: an astounding

- baseline for recognition. In *Proceedings of the IEEE conference on computer vision and pattern recognition workshops*, pages 806–813, 2014. 2
- [21] S. Shojaedini and M. Heidari. A new method for root detection in minirhizotron images: Hypothesis testing based on entropy-based geometric level set decision. *Ijg*, 1(1):1, 2013. 1
- [22] K. Simonyan and A. Zisserman. Very deep convolutional networks for large-scale image recognition. *arXiv preprint arXiv:1409.1556*, 2014. 6
- [23] T. Wang, M. Rostamza, Z. Song, L. Wang, G. McNickle, A. S. Iyer-Pascuzzi, Z. Qiu, and J. Jin. Seg-root: A high throughput segmentation method for root image analysis. *Computers and Electronics in Agriculture*, 162:845–854, 2019. 1
- [24] R. Yasrab, J. A. Atkinson, D. M. Wells, A. P. French, T. P. Pridmore, and M. P. Pound. Rootnav 2.0: Deep learning for automatic navigation of complex plant root architectures. *BioRxiv*, page 709147, 2019. 1
- [25] J. Yosinski, J. Clune, Y. Bengio, and H. Lipson. How transferable are features in deep neural networks? In *Advances in neural information processing systems*, pages 3320–3328, 2014. 2, 9
- [26] G. Yu, A. Zare, H. Sheng, R. Matamala, J. Reyes-Cabrera, F. B. Frischi, and T. E. Juenger. Root identification in minirhizotron imagery with multiple instance learning. 2019. 3
- [27] G. Zeng, S. T. Birchfield, and C. E. Wells. Detecting and measuring fine roots in minirhizotron images using matched filtering and local entropy thresholding. *Machine Vision and Applications*, 17(4):265–278, 2006. 1
- [28] G. Zeng, S. T. Birchfield, and C. E. Wells. Rapid automated detection of roots in minirhizotron images. *Machine Vision and Applications*, 21(3):309–317, 2010. 1
- [29] Y. Zhang, J. Wu, W. Chen, Y. Chen, and X. Tang. Prostate segmentation using z-net. *arXiv preprint arXiv:1901.06115*, 2019. 1
- [30] Y. Zhu, M. Aoun, M. Krijn, J. Vanschoren, and H. T. Campus. Data augmentation using conditional generative adversarial networks for leaf counting in arabidopsis plants. *Computer Vision Problems in Plant Phenotyping (CVPPP2018)*, 2018. 1